

Molecular dynamics modeling of stishovite

Sheng-Nian Luo^{a,*}, Tahir Çağın^b, Alejandro Strachan^b,
William A. Goddard III^b, Thomas J. Ahrens^a

^a *Seismological Laboratory, California Institute of Technology, Pasadena, CA 91125, USA*

^b *Materials and Process Simulation Center, Beckman Institute (139-74), California Institute of Technology, Pasadena, CA 91125, USA*

Received 30 January 2002; received in revised form 24 April 2002; accepted 1 June 2002

Abstract

A Morse-stretch potential charge equilibrium force field for silica system has been employed to simulate the thermodynamics of stishovite with the molecular dynamics (MD) method. The equation of state, thermal expansivity and melting curve of stishovite have been obtained. This simple force field yielded results in accordance with the static and dynamic experiments. The stishovite melting simulation appears to validate the interpretation of superheating of the solid along the Hugoniot in the shock melting experiments. MD simulations show that the thermal expansivity of stishovite at lowermost mantle conditions is a weak function of temperature. The phase diagram of silica up to the mega bar regime is proposed based on the experimental and theoretical studies. The related physical and geophysical implications are addressed. © 2002 Elsevier Science B.V. All rights reserved.

Keywords: thermodynamic properties; equations of state; stishovite; silica; melting

1. Introduction

Silica is important not only as a main constituent of the Earth and other terrestrial planets but also as a model system to study the fundamental physics of material properties, such as phase changes and interatomic potentials. Stishovite-type phase is geophysically important due to its wide range of stability in the mantle, the possible chemical reactions of silicates with liquid Fe at the core–mantle boundary (CMB) [1] and its presence in impact craters [2] and meteorites [3]. To

interpret the seismic structure of the Earth in terms of chemical composition, and understand the transport processes (e.g. heat and mass) associated with the issues such as Earth dynamics and evolution, the knowledge of thermodynamics of SiO₂ as an end member of the MgO–SiO₂ system is crucial. Various experimental studies such as diamond-anvil cell (DAC) and shock wave experiments have shown that silica undergoes polymorphic phase changes and amorphization when subjected to high pressure (P) and temperature (T) [4], but its properties at PT conditions of the Earth's interior and during impact are not well constrained. Complementary to experiments, first-principle and molecular dynamics (MD) methods have been applied to the silica system (e.g. [5–7]), while the latter has the advantage to

* Corresponding author.

Tel.: +1-626-395-3825; Fax: +1-626-564-0715.

E-mail address: sluo@gps.caltech.edu (S.-N. Luo).

handle longer dynamic simulations and larger system sizes required by processes such as phase changes. One interesting challenge in MD modeling is to develop simple theories that accurately describe interatomic interactions and hence material properties. The Morse-stretch potential charge equilibrium force field (MS-Q FF) has been developed to predict the phase changes in ionic insulators such as minerals and ceramics. The proposed MS-Q FF for silica system describes both the four-fold and six-fold coordinated systems, silica glass and pressure-induced phase changes [8]. In this paper, we will apply the MS-Q FF for silica to simulate the equation of state (EOS), thermal expansivity and melting of stishovite and discuss the possible physical and geophysical implications.

2. MD simulation method

MD methods utilize a parameterized analytical force field obtained by fitting to either experimental or first-principle results, from which the atomic motions are calculated from Newtonian physics and thermodynamic properties from statistical mechanics [9–12]. Various potentials for the SiO₂ system have been proposed (e.g. [6]) and cross-checking is necessary. The application of MS-Q FF to silica describes well the general behavior of the SiO₂ system [8] despite of its simplicity. The MS-Q FF includes non-electrostatic (Morse-stretch potential) and electrostatic (evaluated from instantaneous charge equilibrium) contributions.

The non-electrostatic interactions are represented by a simple two-body Morse-stretch (MS) potential:

$$U_{ij}^{\text{MS}}(R_{ij}) = D_0 \left[e^{-\gamma(1-R_{ij}/R_0)} - 2e^{\frac{\gamma}{2}(1-R_{ij}/R_0)} \right] \quad (1)$$

where R_{ij} is the interatomic distance and the MS parameters D_0 , R_0 and γ for Si–Si, O–O and Si–O were optimized from experimental results and listed in Table 1. The electrostatic contribution to force field is evaluated from the charges on the atoms of the instantaneous configuration, i.e. the charges are not fixed during dynamics. For different geometric configuration, the charge equilibrium (QEq) procedure is applied to compute charges by requiring that the chemical potential χ_A is equal on all A atoms (similar for B) [8,13]. χ_A is a function of the charges (Q_i) on all the atoms of the system and the distance R_{AB} between A and B:

$$\chi_A(Q_1, \dots, Q_N) = \chi_A^0 + J_{AA}^0 Q_A + \sum_{B \neq A} J_{AB}(R_{AB}) Q_B \quad (2)$$

and $J_{AB}(R)$ is described as a shielded Coulomb potential for a normalized ns Slater orbital with the orbital exponent given by R_A and R_B , the atomic radii at the standard state [13]. The atomic parameters χ^0 , J^0 , R_A and R_B for Si and O are listed in Table 1. Thus, the electrostatic contribution can be evaluated from the charges by the QEq procedure at each time step of the dynamics.

Given the MS-Q FF, classical MD can be em-

Table 1
MS-Q FF parameters for SiO₂[8]

Morse-stretch parameters:	R_0 (Å)	D_0 (kcal/mol)	γ
O–O	3.7835	0.5363	10.4112
Si–Si	3.4103	0.2956	11.7139
Si–O	1.6148	45.9970	8.8022
QEq parameters for O and Si:	χ^0 (eV)	J^0 (eV)	R (Å)
O	8.741	13.364	0.669
Si	4.168	6.974	1.176

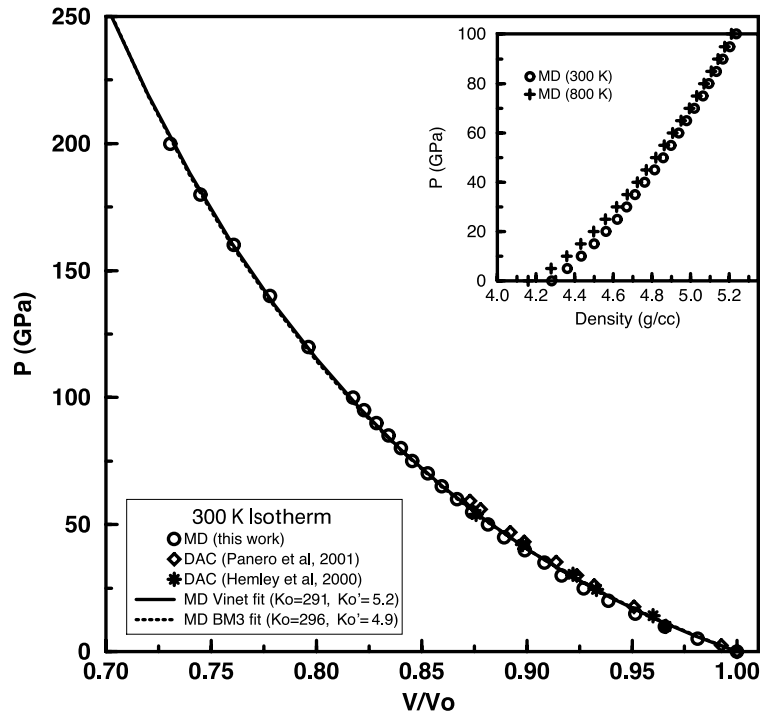


Fig. 1. The 300 K isotherms of stishovite from NPT MD simulation and DAC experiment. V_0 is the ambient specific volume (46.61 \AA^3 per unit cell). The MD results are fitted to Vinet EOS ($K_0 = 291 \text{ GPa}$ and $K'_0 = 5.2$) and the third order Birch–Murnaghan EOS (BM3, $K_0 = 296 \text{ GPa}$ and $K'_0 = 4.9$). (Insert) The 300 K and 800 K isotherms from MD simulations.

ployed to simulate the mechanical and thermodynamic properties of materials subjected to various P and T with different statistical ensembles [11].

3. Simulation results

3.1. EOS of stishovite

The isothermal EOS for stishovite is calculated with isothermal–isobaric MD (NPT ensemble) with a Hoover thermostat [14] and a Rahman–Parrinello barostat [15]. In NPT MD simulations, the Coulombic interactions were evaluated using Ewald summation with real space cutoffs $5\text{--}8 \text{ \AA}$ and reciprocal space cutoffs $0.8\text{--}0.5 \text{ 1/\AA}$ while the Morse interactions were truncated at $R = 0.9 \text{ \AA}$. The integration time step was 1 fs. As pointed out before, the atomic charges depend on the instantaneous configuration of the system and were

updated every 50 time steps. For 300 K isotherm, we conducted a continuous NPT run with progressive pressure increase on a supercell of 672 atoms ($4 \times 4 \times 7 = 112$ unit cells) with three-dimensional (3-D) periodic boundaries. The loading rate is 0.25 GPa/ps in the range of $0\text{--}100 \text{ GPa}$ and 1 GPa/ps in the range of $100\text{--}220 \text{ GPa}$. For a 20 ps run at each pressure, the first 6 ps was taken as thermalization and the remaining 14 ps for statistical averages of lattice parameters and volume. The results are shown in Fig. 1. At given P , the density difference between MD and DAC results [16,17] up to 55 GPa is within 1%. The MD simulation points were fitted to Vinet universal EOS [18,19]:

$$P(x) = 3K_{T0}(1-x)x^{-2}\exp\left[\frac{3}{2}(K'_{T0}-1)(1-x)\right] \quad (3)$$

and the third order Birch–Murnaghan (BM3)

Table 2
EOS parameters for stishovite ($P=0$)

	V_0 (\AA^3)	K_{T0} (GPa)	K'_{T0}
This work, 300 K	46.611	291.1 ± 3.2^a ; 296.4 ± 3.7^b	5.2 ± 0.1^a ; 4.9 ± 0.1^b
This work, 800 K	47.987	222.0 ± 3.8^a ; 225.6 ± 4.4^b	6.1 ± 0.2^a ; 5.8 ± 0.2^b
Brillouin scat. ^c , 300 K	46.581^d	313 ± 4	–
Ultrasonic ^e , 300 K	–	305 ± 5	5.3 ± 0.1
DAC ^f , 300 K	–	312.9 ± 3.4	4.8 ± 0.2
DAC ^g , 300 K	46.615	298 ± 8	3.98 ± 0.46
Shock wave ^h	46.366	306 ± 5	5.0 ± 0.2

^a Vinet fit.

^b BM3 fit.

^c Weidner et al. [21].

^d Equivalent volume converted from reported density.

^e Li et al. [36].

^f Panero et al. [17].

^g Hemley et al. [4] and references therein.

^h Corrected to 300 K, Luo et al. [37].

EOS [20]:

$$P(f) = 3K_{T0}f(1 + 2f)^{\frac{5}{2}} \left[1 + \frac{3}{2}(K'_{T0} - 4)f \right] \quad (4)$$

where P is pressure, the Eulerian strain $f = 1/2[(V/V_0)^{-2/3} - 1]$, $x = (V/V_0)^{1/3}$, V_0 , K_{T0} and K'_{T0} are the ambient volume, isothermal bulk modulus and its pressure derivative. The values of K_{T0} and K'_{T0} fitted to Vinet EOS and BM3 EOS are very similar and close to experimental results (Table 2). Similarly, the 800 K isotherm is also obtained (Fig. 1, insert, and Table 2) and we can see the softening of the bulk modulus when T is increased from 300 to 800 K.

Table 3
Elastic constants of stishovite ($P=0$)

C_{ij} (GPa)	This Work	Ab initio ^a	Brillouin scattering ^b
C_{11}	478.7	462	453 ± 4
C_{33}	748.0	734	776 ± 5
C_{44}	208.6	255	252 ± 2
C_{66}	157.9	324	302 ± 3
C_{12}	135.9	210	211 ± 5
C_{13}	220.2	195	203 ± 4
K	306.2	312	316 ± 4
μ	191.5	226	220 ± 3

^a Karki et al. [7].

^b Weidner et al. [21].

We calculated the elastic constants C_{ij} of stishovite with the MS-Q FF using analytical second derivatives of the energy with respect to strain at zero temperature and pressure. Table 3 compares our calculated values with ab initio [7] and experimental results [21]. The C_{ij} 's from the MS-Q FF, ab initio calculations and Brillouin scattering are in reasonable agreement. The bulk modulus (K) and shear modulus (μ) were obtained from the stiffness and compliance matrices with the Voigt–Reuss–Hill method [22].

From Fig. 1, Tables 2 and 3, we can see that the MS-Q FF for silica accurately predicts the EOS of stishovite.

3.2. Thermal expansivity of stishovite

While the direct measurement of thermal expansivity is non-trivial, thermal expansivity α can be calculated from MD simulations. To calculate $\alpha(P)$, we performed NPT MD simulations at $P=0$ GPa and $P=120$ GPa, the latter pressure chosen to address the lowermost mantle conditions. The system size is 672 atoms and the heating rate is 2 K/ps. For each T , the first 5 ps was used for thermalization and the last 20 ps for calculating the statistical average of lattice parameters. The linear (α_l) and volume expansivity (α_v) can be computed with:

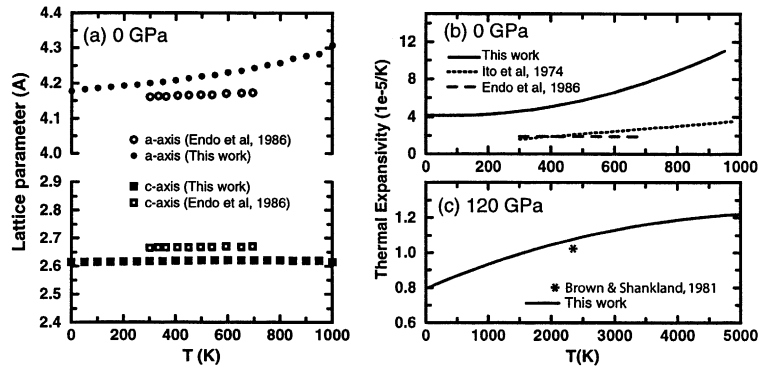


Fig. 2. (a) Comparison of stishovite lattice parameters from MD (this work) with experimental work at 0 GPa [38]. (b) The volume thermal expansivity of stishovite at 0 GPa from this work and experiments [38,39]. (c) The volume thermal expansivity of stishovite at 120 GPa from this work and the calculations for the lower mantle based on seismic observations (star, [33]).

$$\alpha_X = \frac{1}{X} \left. \frac{\partial X}{\partial T} \right|_P \quad (5)$$

where X is either a lattice parameter or volume (V).

Fig. 2a shows the lattice parameters along the $P=0$ isobar from MD simulations as well as experimental data for comparison. While the lattice parameter c from MD is slightly smaller than that from the experiment, the corresponding linear expansivities (α_c) agree. Along a and b axes, MD simulations yielded larger lattice parameters and linear expansivities. Hence, there is a factor of 2 difference in the volume thermal expansivity for $P=0$ at 300 K between MD simulation and experiments, and larger at higher temperatures

(Fig. 2b). This could be due to the overestimated anharmonicity in the force field, or the experimental uncertainties caused by the metastability of stishovite at zero pressure. Similarly, the volume thermal expansivity at $P=120$ GPa is obtained as a weak function of temperature (Fig. 2c). At higher pressures, the anharmonicity is less pronounced and the estimation of α_V at $P=120$ GPa is reasonable.

3.3. The melting curve of stishovite

Stishovite melting at high pressures has been investigated with techniques such as shock temperature measurements [23] and DAC experiments [24]. It is still challenging to determine the phase diagram at high pressures from static and

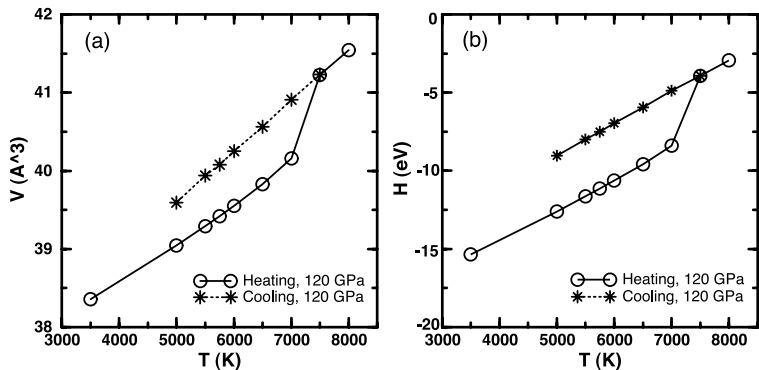


Fig. 3. The single-phase simulation of stishovite melting at 120 GPa. (a) The unit cell (two SiO₂ formulae) volume (V) and (b) the corresponding enthalpy (H) during the heating–cooling process.

dynamic experiments. Complementary to experiments, MD simulations have been employed to tackle this issue [6] but uncertainties remain. Accurate determination of a phase boundary by MD simulations is non-trivial. There are several methods employed to serve this end: single- and two-phase methods [6,25], the thermodynamic integration method [11] and integration of the Clausius–Clapeyron equation [12]. Each method has its own disadvantages and advantages. In this study, we will explore single- and two-phase simulations.

Continuous MD single-phase simulations were conducted on a system of 112 unit cells (672 atoms) with NPT ensemble at different pressures. For each run, the 3-D periodic boundary conditions were applied. The heating and cooling rates were in the range of 12.5–40 K/ps with finer rates at high temperatures. The run time is 20 ps and volume is obtained from the last 15 ps of the single-phase dynamics. Fig. 3 is a typical example ($P=120$ GPa) of single-phase simulation. The volume per unit cell increases steadily during heating until 7000 K, where a sharp increase of the slope (dV/dT) occurs, indicating the initiation of melting, i.e. the melting temperature T_m at 120 GPa is 7000 K. Above 7500 K, the liquid volume increases steadily. The cooling of the system from 8000 K is conducted at the same rate as the heating. The heating–cooling is reversible above 7500 K. Below 7500 K, the hysteresis effect appears: the liquid does not solidify, instead, decreases its volume steadily. The liquid could crystallize eventually at lower temperatures and thus a hysteresis loop may form. The corresponding enthalpy of

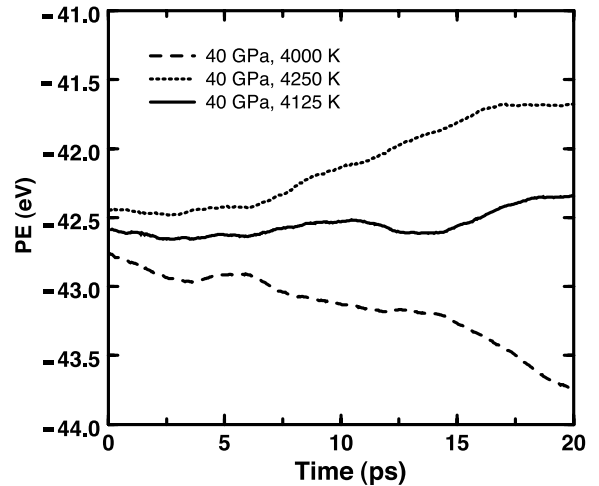


Fig. 4. The dynamics of the PE of the two-phase system ($P=40$ GPa) at different temperatures. The energy is for two SiO_2 formulae.

the same system during the heating–cooling process is shown in Fig. 3b, where a similar hysteresis effect is observed as expected. The slope of the melting curve at a certain pressure, dT/dP , can be obtained from the differences of specific volume (V) and enthalpy (H) between solid and liquid at temperatures near T_m using the Clausius–Clapeyron equation:

$$\frac{dT}{dP} = \frac{T\Delta V}{\Delta H} \quad (6)$$

By repeating the same procedure at different pressures, we obtained the melting point and the melting curve slope (dT/dP) at pressures 20–120 GPa from single-phase simulation (Table 4). Decreas-

Table 4
Melting point of stishovite

P (GPa)	T_m^a (K)	T_m^b (K)	ΔH^c (eV)	ΔV^c (\AA^3)	dT/dP^c (K/GPa)
20	3125 ± 125	3625	3.20	7.3901	50.5
40	4125 ± 125	4500	3.51	4.2025	33.6
60	4625 ± 125	5500	3.34	2.4743	25.4
80	4900 ± 125	6000	3.16	1.4176	16.8
120	5437.5 ± 75	7000	3.52	0.7523	9.3

^a Two-phase simulation.

^b Single-phase simulation, with uncertainties between 250 and 500 K.

^c Calculated from single-phase simulation.

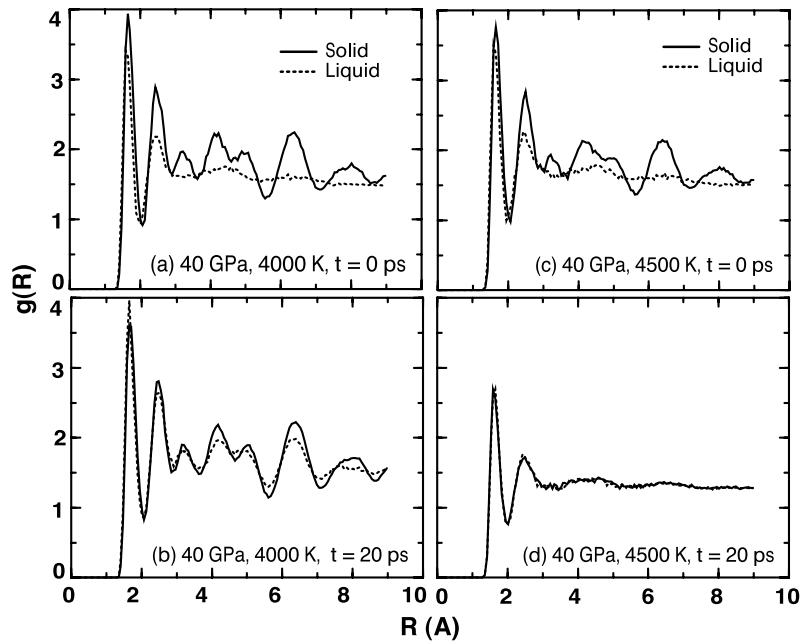


Fig. 5. Snapshots of the RDFs for the atoms originally existing as liquid and solid respectively in the two-phase system at 40 GPa and different temperatures. (a) $T=4000$ K, 0 ps; (b) $T=4000$ K, 20 ps; (c) $T=4500$ K, 0 ps and (d) $T=4500$ K, 20 ps.

ing dT/dP indicates that the melting curve flattens with the increasing pressure.

Single-phase simulation could lead to hysteresis effect as in Fig. 3, i.e. superheating of solid and undercooling of liquid due to the existence of kinetics during the simulation [10,12], especially at high pressures. Thus, the melting point T_m could be overestimated seriously at high pressures we are interested in. The superheating could be circumvented by the thermodynamic integration method [11] or two-phase simulation technique [6,25]. The latter is simpler in physics as well as in computation and widely used. The two-phase simulation models are constructed by combining the solid and liquid models at the same pressure and temperature from the single-phase simulations. Nucleation could be a problem if one tries to crystallize (or melt) the single-phase liquid (or solid), but the two-phase simulation has the advantage that the planar initial solid–liquid interface corresponds to an infinite nucleation, much larger than the required critical radius.

To construct the starting model for the two-phase simulation, stishovite liquid and solid mod-

els at the same P and T from the single-phase simulations were placed into a supercell with 3-D periodic boundaries. The system size is 672×2 atoms, twice that for single-phase simulations. One concern in combining solid and liquid models is the solid–liquid interface: while the total free energy of the two-phase system should be minimum, the internal pressure should remain unchanged when adjusting the interface thickness to minimize the energy. The tradeoff between interface thickness and the corresponding internal pressure changes complicates the simulation: the internal pressure could vary by an appreciable amount with the interface thickness, thus the melting temperature could be over- or underestimated if the pressure change is not relaxed. When constructing the two-phase model, the interface thickness was adjusted to keep internal pressure equal to the nominal pressure. This issue could be bypassed with a larger system.

With the two-phase model constructed at a certain temperature and fixed pressure, NPT MD runs were conducted to bracket the melting point by varying T . If the temperature is higher than the

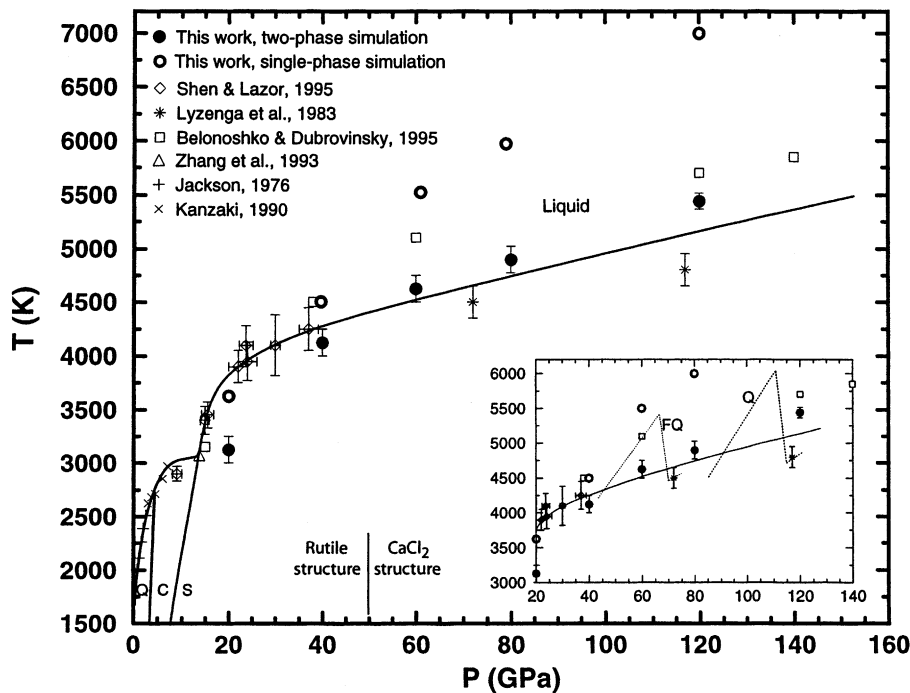


Fig. 6. The melting curve of stishovite and phase diagram of silica system from this work and former experimental and theoretical studies [23,24,26–28]. Q: quartz; C: coesite; S: stishovite and FQ: fused quartz. (Insert) Dashed lines are shock temperature measurement of shocked fused quartz and quartz [23]. The sharp drop of temperature indicates the melting of stishovite. The portion of Hugoniot above the melting curve (solid line) is the superheated stishovite solid.

melting temperature, T_m , the two-phase system should become liquid eventually and the opposite when $T < T_m$. If the NPT run is conducted at T_m , the system should remain unchanged. Thus the melting point is bracketed. There are several ways to determine if the system is melted, crystallized or remains unchanged. One is the direct visualization by plotting the two-phase model. The temperature effect on the system can also be obtained from potential energy (PE) and radial distribution function (RDF). Fig. 4 shows the PE dynamics of a two-phase system at 40 GPa simulated at different temperatures. At $T = 4250$ K, PE increases with time, suggesting that the solid is melting thus $T_m < 4250$ K. The opposite is for $T = 4000$ K. At $T = 4125$ K, PE remains almost constant for the 20 ps run, suggesting the T_m is close to 4125 K. Melting and crystallizing can also be identified from the long-range order manifested in RDFs. RDF is the spherically averaged distribution of interatomic vector lengths and can be

computed from the trajectory file data. Fig. 5a shows the RDFs of all the Si and O atoms in solid (solid line) and in liquid (dashed line) at the beginning of the two-phase NPT run ($t = 0$ ps) at 40 GPa and 4000 K. The first peak is Si–O and the second Si–Si. The solid RDF has distinct peaks up to the cutoff distance (9 Å) due to the long-range order of crystalline solid, while the liquid RDF has only the first two peaks and lacks long-range order as expected. When this two-phase model evolves from $t = 0$ ps to $t = 20$ ps, long-range order becomes apparent in the liquid half of the two-phase system, suggesting that at 4000 K the liquid crystallizes. Within 20 ps, the liquid reaches a RDF similar to the solid portion (Fig. 5b). Thus we found that at 40 GPa, the melting temperature $T_m > 4000$ K. The opposite happens for $T = 4500$ K where the solid loses its long-range order and melts, i.e. $T_m < 4500$ K (Fig. 5c,d). Thus T_m is bracketed between 4000 and 4500 K.

By repeating the above procedure, the melting temperature T_m at certain pressure can be bracketed, in our case, with variations less than 125 K. The melting points for stishovite at five different pressures are shown in Table 4. By comparing the melting temperatures T_m from the single- and two-phase simulations, we found that the latter yielded lower T_m by 500–1500 K. At high pressure, the difference is more pronounced. The melting curve flattening from the two-phase simulations is consistent with the Clausius–Clapeyron slope changes from the single-phase simulations.

Fig. 6 shows our MD results (closed and open circles) along with the results from static and dynamic experiments and former MD simulations on stishovite. The single-phase simulations yielded results close to the DAC results [24] at 20 and 40 GPa, but significantly higher results above 40 GPa than those from shock wave experiment [23] and former MD modeling [6]. This indicates that single-phase simulation could lead to more pronounced superheating at high pressures. But at low pressures, single-phase simulation might produce reasonable results. Our two-phase simulation results are in reasonably good agreement with former DAC and shock melting studies, except at 20 GPa where the large slope of the melting curve makes the simulation more sensitive to the interface effect discussed above. Comparing with former MD simulation, our two-phase simulation results are lower and closer to experiments except at 20 GPa.

The melting curve of stishovite is proposed based on our MD simulations and former DAC and shock wave experiment results from 20 to 120 GPa. The phase boundaries for silica at low pressures are established based on former static experiments [26–28]. Thus, the phase diagram of the silica system has been extended to the megabar regime with sound experimental and theoretical bases.

4. Discussion

The MD simulations of the melting curve of stishovite with MS-Q FF are in general agreement with static and dynamic experiments. One signifi-

cance is that it appears to validate the interpretation of superheating of solid along the Hugoniot from shock melting experiments (Fig. 6 insert, the dashed portion above the solid line) on fused quartz and quartz proposed by Lyzenga et al. [23]. Superheating of shocked solid might also be common to iron [29] and other materials. The first liquid states on the Hugoniot (stars, Fig. 6) are close to the melting curve although undercooling might exist.

The silica phase diagram and EOS will help constrain the interpretation of the seismic structure in terms of the chemical composition of the Earth's interior, such as the chemical reactions at the CMB which might give rise to the lateral heterogeneity at D'' [1]. In particular, the possibility that the ultra-low velocity zone ([30,31]) at the CMB is caused by partial melting [30] demands that we develop a basis for modeling curves and EOS data for solids and liquids in the MgO–SiO₂–FeO–Fe system, at least.

Although most cosmochemical models call for a perovskite plus magnesiowustite lower mantle, physical data permit considerable free silica. Thus, e.g., it has been shown that the mean atomic weight μ is constant and close to 21 throughout the lower mantle [32]. For silica, μ is 20. Seismic results show that the thermal expansivity in the lowermost mantle is close to $1 \times 10^{-5}/\text{K}$ (e.g. at 2671 km depth and 2405 K, [33]), close to our simulations at 120 GPa (about 2671 km depth in the Earth, Fig. 2c). Our results have shown that at lower mantle condition, thermal expansivity of stishovite is a weak function of temperature, which may be true more generally for lower mantle phases and for the bulk lower mantle. The knowledge of thermal expansivity can help to constrain other important parameters such as the Grüneisen parameter and Rayleigh number.

It is significant that a simple force field, the MS-Q FF for silica system, leads to results in accordance with previous experimental and theoretical studies considering the fact that this force field describes the whole silica system with complex polymorphic phase changes. But discrepancies exist. This MS-Q FF predicts the CaCl₂ transition at ~ 130 GPa and α -PbO₂ transition at

~102 GPa from energy minimization simulations. While the latter transition pressure is in good agreement with ab initio results (compared to 98 [7]), our force field overestimates the free energy of the CaCl₂ phase leading to a high transition pressure compared with previous results (~50 GPa) from experiments and ab initio calculations [7,34]. This could be due to the simplicity of the potential which fails to accurately describe the subtle structural and energetic differences between the rutile and CaCl₂ structure. Although our potential predicts the transition to the orthorhombic structure at too high a pressure, the high-pressure melting temperature calculations remain relevant since stishovite and the higher pressure phases have similar properties. Ab initio calculations [7,35] and experimental results [34] show that the shear modulus is only significantly reduced at the CaCl₂ transition pressure (~50 GPa). The comparisons between elastic constants for rutile, orthorhombic and columbite (α -PbO₂) as a function of pressure show the same trend across the different phases except in a narrow pressure region around ~50 GPa [7].

5. Conclusion

We have applied a Morse-stretch charge equilibrium force field for silica system to stishovite and obtained EOS, thermal expansivity and melting curve of stishovite. The simulations are in general agreement with previous experimental and theoretical studies, and confirm extrapolation using standard EOS formulisms. The thermal expansivity of silica at lowermost mantle conditions is a weak function of temperature. The stishovite melting simulation appears to validate the interpretation of superheating of the solid along Hugoniot. The EOS and phase diagram of silica will help to constrain the interpretation of the seismic observations and geodynamic modeling of the mantle.

Acknowledgements

S.-N.L. has been supported by NSF grants

(T.J.A.). The computational facility is supplied by MSC, Beckman Institute, Caltech (W.A.G.). The constructive comments by P. Asimow and two anonymous reviewers helped to improve the manuscript. Contribution No. 8858, Division of Geological and Planetary Sciences, California Institute of Technology. [RV]

References

- [1] E. Knittle, R. Jeanloz, Earth's core–mantle boundary: results of experiments at high pressures and temperatures, *Science* 251 (1991) 1438–1443.
- [2] E.C.T. Chao, J.J. Fahey, J. Littler, D.J. Milton, Stishovite, a new mineral from Meteor Crater, *J. Geophys. Res.* 67 (1962) 419–421.
- [3] A. ElGoresy, L. Dubrovinsky, T.G. Sharp, S.K. Saxena, M. Chen, A monoclinic post-stishovite polymorph of silica in the Shergotty Meteorite, *Science* 288 (2000) 1632–1634.
- [4] R.J. Hemley, C.T. Prewitt, K.J. Kingma, High-pressure behavior of silica, *Rev. Mineral.* 29 (1994) 41–81.
- [5] R.E. Cohen, First-principle theory of crystalline SiO₂, *Rev. Mineral.* 29 (1994) 369–402.
- [6] A.B. Belonoshko, L.S. Dubrovinsky, Molecular dynamics of stishovite melting, *Geochim. Cosmochim. Acta* 59 (1995) 1883–1889.
- [7] B.B. Karki, L. Stixrude, J. Crain, Ab initio elasticity of three high-pressure polymorphs of silica, *Geophys. Res. Lett.* 24 (1997) 3269–3272.
- [8] E. Demiralp, T. Cagin, W.A. Goddard III, Morse-Stretch potential charge equilibrium force field for ceramics: application to the quartz-stishovite phase transition and to silica glass, *Phys. Rev. Lett.* 82 (1999) 1708–1711.
- [9] R.T. Cygan, Molecular modeling in Mineralogy and Geochemistry, *Rev. Mineral. Geochem.* 42 (2001) 1–35.
- [10] M.P. Allen, D.J. Tildesley, *Computer Simulation of Liquids*, Clarendon Press, Oxford, 1987.
- [11] D. Frenkel, B. Smit, *Understanding Molecular Simulation*, Academic Press, 1996.
- [12] A. Strachan, T. Cagin, W.A. Goddard III, Phase diagram of MgO from density-function theory and molecular-dynamics simulation, *Phys. Rev. B* 60 (1999) 15084–15093.
- [13] A.K. Rappe, W.A. Goddard III, Charge equilibration for molecular dynamics simulations, *J. Phys. Chem.* 95 (1991) 3358–3363.
- [14] W.G. Hoover, Canonical dynamics: equilibrium phase-space distributions, *Phys. Rev. A* 31 (1985) 1695–1697.
- [15] M. Parrinello, A. Rahman, Polymorphic transitions in single crystal: A new molecular dynamics method, *J. Appl. Phys.* 52 (1981) 7182–7190.
- [16] R.J. Hemley, J. Shu, M.A. Carpenter, J. Hu, H.K. Mao, K.J. Kingma, Strain/order parameter coupling in the fer-

- roelastic transitions in dense SiO₂, *Solid State Commun.* 114 (2000) 527–532.
- [17] W.R. Panero, L.R. Benedetti, R. Jeanloz, Equation of state of stishovite and interpretation of SiO₂ shock compression data, *J. Geophys. Res.*, submitted
- [18] P. Vinet, J. Ferrante, Compressibility of solids, *J. Geophys. Res.* 92 (B9) (1987) 9319–9325.
- [19] R.E. Cohen, O. Gülseren, R.J. Hemley, Accuracy of equation-of-state formulations, *Am. Mineral.* 85 (2000) 338–344.
- [20] F. Birch, Finite strain isotherm and velocities for single-crystal and polycrystalline NaCl at high pressures and 300 K, *J. Geophys. Res.* 95 (1978) 1257–1268.
- [21] D. Weidner, J.D. Bass, A.E. Ringwood, W. Sinclair, The single-crystal elastic moduli of stishovite, *J. Geophys. Res.* 87 (1982) 4740–4746.
- [22] R. Hill, The elastic behavior of a crystalline aggregate, *Proc. Phys. Soc. London Ser. A* 65 (1952) 349–354.
- [23] G.A. Lyzenga, T.J. Ahrens, A.C. Mitchell, Shock temperatures of SiO₂ and their geophysical implications, *J. Geophys. Res.* 88 (B3) (1983) 2431–2444.
- [24] G. Shen, P. Lazor, Measurement of melting temperatures of some minerals under lower mantle pressures, *J. Geophys. Res.* 100 (B9) (1995) 17699–17713.
- [25] J.R. Morris, C.Z. Wang, K.M. Ho, C.T. Chan, Melting line of aluminum from simulations of coexisting phases, *Phys. Rev. B* 49 (1994) 3109–3115.
- [26] I. Jackson, Melting of the silica isotypes SiO₂, BeF₂ and GeO₂ at elevated pressures, *Phys. Earth Planet. Int.* 13 (1976) 218–231.
- [27] M. Kanzaki, Melting of silica up to 7 GPa, *J. Am. Ceram. Soc.* 73 (1990) 3706–3707.
- [28] J. Zhang, R.C. Liebermann, T. Gasparik, C.T. Herzberg, Y. Fei, Melting and subsolidus relations of SiO₂ at 9–14 GPa, *J. Geophys. Res.* 98 (1993) 19785–19793.
- [29] J.M. Brown, R.G. McQueen, Phase-transitions, Grüneisen-parameter, and elasticity for shocked iron between 77 GPa and 400 GPa, *J. Geophys. Res.* 91 (B7) (1986) 7485–7494.
- [30] E.J. Garnero, D.V. Helmberger, A very slow basal layer underlying large-scale low-velocity anomalies in the lower mantle beneath the Pacific – evidence from core phases, *Phys. Earth Planet. Inter.* 91 (1995) 161–176.
- [31] S.-N. Luo, S. Ni, D.V. Helmberger, Evidence for a sharp lateral variation of velocity at the core–mantle boundary from multipathed PKPab, *Earth Planet. Sci. Lett.* 189 (2001) 155–164.
- [32] J.P. Watt, T.J. Shankland, N. Mao, Uniformity of mantle composition, *Geology* 3 (1975) 92–97.
- [33] J.M. Brown, T.J. Shankland, Thermodynamic parameters in the Earth as determined from seismic profiles, *Geophys. J. R. Astron. Soc.* 66 (1981) 579–596.
- [34] K.J. Kingma, R.E. Cohen, R.J. Hemley, H.-K. Mao, Transformation of stishovite to a denser phase at lower-mantle pressures, *Nature* 374 (1995) 243–245.
- [35] B.B. Karki, L. Stixrude, R.M. Wentzcovich, High-pressure elastic properties of major materials of Earth’s mantle from first principles, *Rev. Geophys.* 39 (2001) 507–534.
- [36] B. Li, S.M. Rigden, R.C. Liebermann, Elasticity of stishovite at high pressure, *Phys. Earth Planet. Int.* 96 (1996) 113–127.
- [37] S.-N. Luo, J.L. Mosenfelder, P.D. Asimow, T.J. Ahrens, Direct shock wave loading of stishovite to 235 GPa: Implications for perovskite stability relative to oxide assemblage at lower mantle conditions, *Geophys. Res. Lett.* (2002) in press.
- [38] S. Endo, T. Akai, Y. Akahama, M. Wakatsuki, T. Nakamura, Y. Tomii, K. Koto, Y. Ito, M. Tokonami, High temperature X-ray study of single crystal stishovite synthesized with Li₂WO₄ as flux, *Phys. Chem. Miner.* 13 (1986) 146–151.
- [39] H. Ito, K. Kawada, S.-I. Akimoto, Thermal expansion of stishovite, *Phys. Earth Planet. Int.* 8 (1974) 227–281.